Chin. Geogra. Sci. 2019 Vol. 29 No. 3 pp. 446–462
https://doi.org/10.1007/s11769-019-1033-3

Springer Science Press
www.springerlink.com/content/1002-0063

Spatial Downscaling of the Tropical Rainfall Measuring Mission Precipitation Using Geographically Weighted Regression Kriging over the Lancang River Basin, China

LI Yungang[1, 2], ZHANG Yueyuan[1, 2], HE Daming[1, 2], LUO Xian[1, 2], JI Xuan[1, 2]

(1. *Institute of International Rivers and Eco-security*, *Yunnan University*, *Kunming* 650091, *China*; 2. *Yunnan Key Laboratory of International Rivers and Transboundary Eco-security*, *Yunnan University*, *Kunming* 650091, *China*)

Abstract: Satellite-based precipitation products have been widely used to estimate precipitation, especially over regions with sparse rain gauge networks. However, the low spatial resolution of these products has limited their application in localized regions and watersheds. This study investigated a spatial downscaling approach, Geographically Weighted Regression Kriging (GWRK), to downscale the Tropical Rainfall Measuring Mission (TRMM) 3B43 Version 7 over the Lancang River Basin (LRB) for 2001–2015. Downscaling was performed based on the relationships between the TRMM precipitation and the Normalized Difference Vegetation Index (NDVI), the Land Surface Temperature (LST), and the Digital Elevation Model (DEM). Geographical ratio analysis (GRA) was used to calibrate the annual downscaled precipitation data, and the monthly fractions derived from the original TRMM data were used to disaggregate annual downscaled and calibrated precipitation to monthly precipitation at 1 km resolution. The final downscaled precipitation datasets were validated against station-based observed precipitation in 2001–2015. Results showed that: 1) The TRMM 3B43 precipitation was highly accurate with slight overestimation at the basin scale (i.e., *CC* (correlation coefficient) = 0.91, *Bias* = 13.3%). Spatially, the accuracies of the upstream and downstream regions were higher than that of the midstream region. 2) The annual downscaled TRMM precipitation data at 1 km spatial resolution obtained by GWRK effectively captured the high spatial variability of precipitation over the LRB. 3) The annual downscaled TRMM precipitation with GRA calibration gave better accuracy compared with the original TRMM dataset. 4) The final downscaled and calibrated precipitation had significantly improved spatial resolution, and agreed well with data from the validated rain gauge stations, i.e., *CC* = 0.75, *RMSE* (root mean square error) = 182 mm, *MAE* (mean absolute error) = 142 mm, and *Bias* = 0.78% for annual precipitation and *CC* = 0.95, *RMSE* = 25 mm, *MAE* = 16 mm, and *Bias* = 0.67% for monthly precipitation.

Keywords: precipitation; Tropical Rainfall Measuring Mission (TRMM) 3B43; Geographically Weighted Regression Kriging (GWRK); spatial downscaling; the Lancang River Basin, China

Citation: LI Yungang, ZHANG Yueyuan, HE Daming, LUO Xian, JI Xuan, 2019. Spatial Downscaling of the Tropical Rainfall Measuring Mission Precipitation Using Geographically Weighted Regression Kriging over the Lancang River Basin, China. *Chinese Geographical Science*, 29(3): 446–462. https://doi.org/10.1007/s11769-019-1033-3

1 Introduction

Precipitation plays a vital role in the global water cycle, affecting energy transfer and maintaining biosphere functions (He et al., 2017; Ma et al., 2017a). As a complex natural phenomenon, precipitation is characterized by significant variability both in time and space (Bohnenstengel et al., 2011). Accurate estimates of pre-

Received date: 2018-03-06; accepted date: 2018-05-27
Foundation item: Under the auspices of the National Natural Science Foundation of China (No. 41661099); the National Key Research and Development Program of China (No. Grant 2016YFA0601601)
Corresponding author: HE Daming. E-mail: dmhe@ynu.edu.cn

cipitation are crucial for a wide range of applications, from hydrology to climate studies (Prakash et al., 2018). However, obtaining accurate precipitation data in mountainous areas remains challenging due to the sparsity of gauge networks and a remarkable spatio-temporal variability in precipitation (Zhou et al., 2017). Conventional gauge observations could provide a relatively accurate point-based measurement of precipitation, but measurements are susceptible to uncertainties, such as evaporative loss, wind effects, and gauge placement (Derin et al., 2016). Moreover, the sparseness of gauge networks is inadequate for capturing the high variability of precipitation over remote mountainous regions (Miao et al., 2015). Therefore, gridded precipitation data obtained using interpolation methods based on gauge observations may not be reliable, especially in those regions with few gauges and complex topography (Ma et al., 2017a; Zhao et al., 2018).

Satellite remote sensing provides global gridded precipitation estimates, which offer new opportunities for more accurate gridded precipitation estimates in regions with limited accessibility and sparse ground-based observations (Michaelides et al., 2009). A series of satellite-based precipitation products with continuous temporal availability and global coverage have been released, such as the Global Precipitation Climatology Project (GPCP) (Huffman et al., 1997), Precipitation Estimation from Remotely Sensed Information using Artificial Neural Networks (PERSIANN) (Sorooshian et al., 2000), Climate Prediction Center (CPC) morphing algorithm (CMORPH) (Joyce et al., 2004), Tropical Rainfall Measuring Mission (TRMM), Multisatellite Precipitation Analysis (TMPA) (Huffman et al., 2007), and Global Precipitation Measurement (GPM) (Hou et al., 2014). Most of these satellite precipitation products have been widely used in various applications (He et al., 2017; Liu et al., 2017; Yuan et al., 2017; Zhang et al., 2018c). However, current satellite-based precipitation products are available only at a spatial resolution of 0.1º or lower, which is still too coarse for hydrological simulation and environmental modeling for specific local basins and regions. Deriving precipitation datasets with fine spatial resolution (e.g., 1 km) from a satellite source remains an important issue.

It is widely acknowledged that there are correlative relationships between precipitation and environmental variables, such as the Normalized Difference Vegetation Index (NDVI), the Digital Elevation Model (DEM), and the Land Surface Temperature (LST) (Li et al., 2002; Jing et al., 2016; Meersmans et al., 2016). Based on the relationships between precipitation and environmental variables, many studies have derived precipitation estimates from satellite precipitation at finer spatial scales using various downscaling models. The most commonly used regression models include the exponential function (Immerzeel et al., 2009), multiple linear regression (Jia et al., 2011; Fang et al., 2013), random forests (Jing et al., 2017), and regression kriging (Teng et al., 2014). However, most previous studies have been conducted based on a global regression model, which assumes that the relationship between the independent variable and the explanatory variables is constant in space. However, the relationship between precipitation and environmental variables is spatially varying and scale-dependent (Foody, 2003). To overcome this limitation, Chen et al. (2014) and Xu et al. (2015) proposed a geographically weighted regression (GWR) model to obtain higher resolution precipitation datasets based on the assumption that the relationship between rainfall-environmental variables varies spatially. Ma et al.(2017b) introduced a spatial data mining algorithm for downscaling TMPA data over China considering non-stationary relationships between precipitation and land surface characteristics at various scales. In addition, satellite precipitation products are subject to regionally and seasonally varying uncertainties associated with systematic and random errors; these errors would be inevitably introduced into downscaled precipitation data (Prakash et al., 2015). Duan and Bastiaanssen (2013) introduced geographical differential analysis (GDA) and geographical ratio analysis (GRA) calibration methods based on the gauge stations data to reduce errors in downscaled precipitation datasets.

Geographically Weighted Regression Kriging (GWRK) is a hybrid technique, and extension of the GWR approach (Kumar et al., 2012). GWR has the advantage of investigating non-stationary and scale- dependent characteristics of the relationship between dependent and explanatory variables (Foody, 2003). Therefore, GWR technique is suitable for exploring and describing complex relationships between precipitation and other environmental variables (Chen et al., 2014). In addition, kriging allows one to capitalize on the spatial correlation between neighboring observations to predict attribute

values at un-sampled locations (Goovaerts, 2000; Lloyd, 2005). Therefore, GWRK composed of GWR and kriging residuals can be used more efficiently for estimating residuals to predict trends (Harris et al., 2010). The GWRK technique has proven to be an effective method for spatial estimation in various applications (Harris et al., 2010; Kumar et al., 2012; Imran et al., 2015; Zhang et al., 2018b).

Previous studies have reported that the TRMM precipitation is able to provide reliable estimations of precipitation in the Lancang-Mekong River Basin, with the potential for drought monitoring and hydrological simulations (Zeng et al., 2012, 2013; Lauri et al., 2014; Wang et al., 2016; He et al., 2017). Therefore, the aim of this study was to investigate the application of the GWRK method in downscaling the TRMM 3B43 V7 data over the Lancang River Basin (LRB). The main objectives were to: 1) evaluate the accuracy of the TRMM 3B43 precipitation data; 2) map annual precipitation at 1 km resolution based on the GWRK downscaling algorithm and the GRA calibration method; and 3) disaggregate the annual downscaled and calibrated precipitation into monthly precipitation using a simple fraction disaggregation method. This study provides precipitation estimates with high spatial resolution for hydrology research and water resources management purpose, and contributes to the knowledge regarding the spatial downscaling methodology of satellite-based precipitation products in mountainous areas without sufficient rainfall measurement.

2 Materials and Methods

2.1 Study area

The LRB is located in Southwest China, between 94° E–102° E and 21° N–34° N (Fig. 1). The river is 2160 km in length and the basin area is approximately 16.48×10^4 km^2 (He et al., 2007c). The elevation of the catchment ranges from 499 to 6334 m above mean sea level, decreasing from north to south. The geomorphology of the basin varies from high mountains and deep valleys, which run in a north-south direction, to medium/low mountains and wide valleys (He et al., 2005). The terrain variability, coupled with the influences of the Indian and East Asian monsoons, results in complex spatio-temporal variations in precipitation. The annual average precipitation is approximately 970 mm, ranging

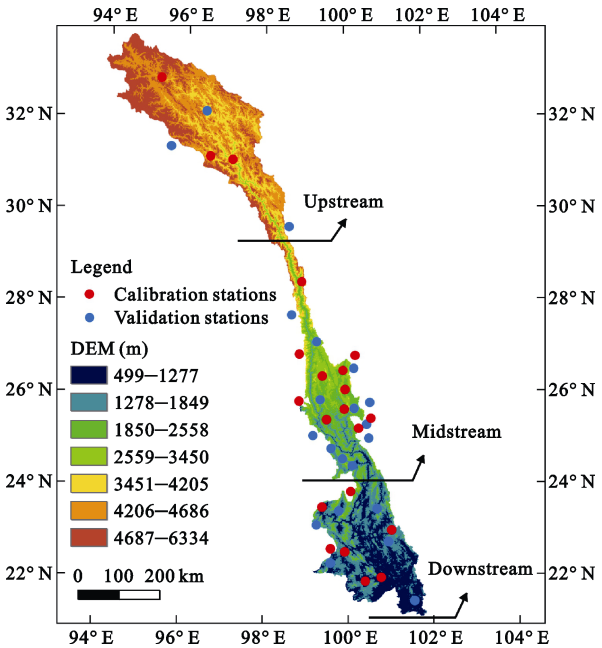

Fig. 1 Location and elevation of the meteorological stations of the Lancang River Basin in southwestern China; DEM, Digital Elevation Model

from 850 mm to 1100 mm, with 80% of the annual rainfall occurring during the rainy season (May to October) (Shi et al., 2013). Spatially, the annual precipitation is more than 2000 mm in the southeast region while less than 500 mm in the northwest region. The complex climate conditions and terrain features have resulted in a rich biodiversity across the LRB (He et al., 2007a). Vegetation in the upstream region consists of temperate alpine meadow, temperate coniferous forest, and temperate deciduous broad-leaved forest. The midstream region is temperate, consisting of subtropical high deciduous shrub, sparse grassland, semi-evergreen seasonal forest, and wet evergreen broad-leaved forest. Tropical, subtropical evergreen broad-leaved forest, tropical rain forest, and scattered deciduous forest are found in the downstream region (Zhang et al., 2015).

2.2 Data

Monthly precipitation data from 42 rain gauge stations (RGS) for 2001–2015 were obtained from the China Meteorological Data Service Center (CMDC) (http://data.cma.cn) and the Meteorological Agency of Yunnan Province (MAYP). The quality of the dataset has been checked by the CMDC and MAYP. We also performed routine quality assessment including statistical tests, visual data plots and histograms, to ensure there were no

missing or erroneous records. The locations of the 42 rain gauges are shown in Fig. 1; stations are densely distributed in downstream and midstream regions and relatively sparse in upstream. The altitudes of the stations ranged from 556 m to 4172 m with 88% above 1000 m.

The TRMM is a joint project of the National Aeronautics and Space Administration (NASA) and the Japan Aerospace Exploration Agency (JAXA) launched on the 27 November 1997, with the goal of monitoring and studying rainfall in tropical and subtropical regions. The TRMM Multi-satellite Precipitation Analysis (TMPA) was designed to combine all available precipitation datasets from different satellite sensors and monthly surface rain gauge data to provide a 'best' estimate of precipitation covering the global region between 50° N and 50° S at a resolution of 0.25°(Huffman et al., 2007). For this study, the latest version 7 of the TRMM 3B43 precipitation data, spanning 2001 to 2015, was obtained from http://mirador.gsfc.nasa.gov. The monthly precipitation data were combined to generate the TRMM annual precipitation.

The Terra Moderate Resolution Imaging Spectroradiometer (MODIS) monthly composite NDVI data at 1 km resolution (MOD13A3), spanning the period from January 2001 to December 2015, were downloaded from the NASA Land Processes Distributed Active Archive Center (https://lpdaac.usgs.gov/dataset_discovery/modis). We aggregated the MOD13A3 monthly data into an annual NDVI from 2001 to 2015. The land use dataset (MCD12Q1) was used to identify NDVI outliers caused by factors other than precipitation. Due to a mismatch in spatial resolutions between MOD13A3 and MCD12Q1 datasets, the MCD12Q1 dataset was upscaled to 1 km resolution. We identified anomalous NDVI pixels simply by land use type: pixels categorized as water, wetland, urban, cropland, snow/ice, and barren were identified as anomalies. The detected anomalous pixels were excluded from the original NDVI dataset and then replaced with interpolated values using the IDW method to generate an optimized NDVI dataset (Zhou et al., 2017). The MODIS LST products (MOD11A2) at 1 km resolution from January 2001 to December 2015 were used in this study. MOD11A2 is composed of daytime and nighttime temperature variables (LSTs) at a time interval of eight days. The annual average LSTs were calculated by averaging each 8-day LST. The DEM data were obtained from the NASA Shuttle Radar Topographic Mission (SRTM) (http://srtm.csi.cgiar.org).The DEM with a resolution of 90 m was re-sampled to 1 km using the pixel averaging method. The slope, aspect, and geolocation (longitude and latitude) were further extracted from the DEM.

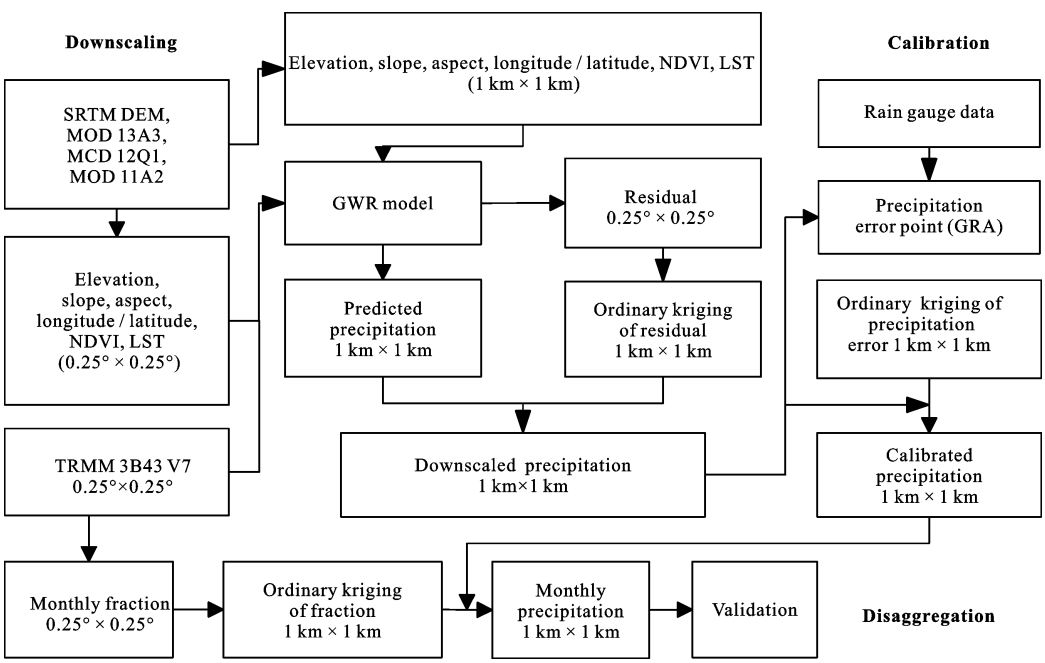

Fig. 2 Flow chart of the downscaling-calibration approach used in the study. NDVI, Normalized Difference Vegetation Index; LST, Land Surface Temperature; SRTM, Shuttle Radar Topographic Mission; DEM, Digital Elevation Model; TRMM, Tropical Rainfall Measuring Mission; GWR, Geographically Weighted Regression; GRA, Geographical ratio analysis

2.3 Methods

A flowchart is provided in Fig. 2 to illustrate the primary steps in the downscaling and calibration process and the monthly fraction disaggregation algorithm.

2.3.1 Downscaling of TRMM 3B43 precipitation

The downscaling method is based on two assumptions: precipitation has a spatial relationship with environmental variables, and this relationship can be addressed using the established model, and that the low resolution model can be used to predict the precipitation at fine resolution with a higher resolution environmental variables dataset (Jing et al., 2016). The specific steps used for downscaling in this study were as follows:

(1) The original NDVI, LST, elevation, slope, and aspect of 1 km resolution were re-sampled at a resolution of 0.25° using a pixel averaging method with the geographical coordinates of the center of each 0.25° grid also being extracted.

(2) The relationships between the re-sampled independent variables and the TRMM 3B43 precipitation data were established using GWR model at the 0.25° scale.

(3) Geolocations along with 1 km spatial resolution variables were entered into the model established in step (2), and downscaled precipitation at 1 km spatial-resolution was obtained.

(4) The difference between the estimated precipitation and the TRMM 3B43 precipitation at the 0.25° scale was calculated, followed by ordinary kriging interpolation into the residuals at 1 km resolution. These residuals were considered as the amount of precipitation that cannot be predicted by the regression model selected in step (3).

(5) The final downscaled precipitation results were obtained by adding the residual correction term to the downscaled precipitation at 1 km resolution.

2.3.2 Geographically Weighted Regression Kriging (GWRK) Model

The GWR model is an extension of traditional standard regression techniques such as ordinary least squares but it allows local rather than global parameter estimates (Fotheringham et al., 2002). The GWR model extends the conventional global regression by adding a geographical location parameter (Gao et al., 2012), and the GWR model can be rewritten as follows (Foody, 2003; Gao et al., 2012; Xu et al., 2015):

$$y_i = \beta_0(u_i, v_i) + \sum_{k=1}^{p} \beta_k(u_i, v_i) x_{ik} + \varepsilon_i \quad i = 1, 2, \cdots, n \tag{1}$$

where y_i, x_{ik} and ε_i are, respectively, dependent variable, kth explanatory variable, and the random error at location i; (u_i, v_i) is the x-y coordinate of ith location; $\beta_0(u_i, v_i)$ represents the intercept at location i, $\beta_k(u_i, v_i)$ represents the local parameter estimate for explanatory variable x_k at location i; n and p are the total number of location and explanatory variable, respectively.

The regression parameters can be estimated by solving the following matrix equation (Foody, 2003; Gao et al., 2012; Xu et al., 2015):

$$\hat{\beta}(u_i, v_i) = (x^T (W(u_i, v_i)) x)^{-1} x^T W(u_i, v_i) y \tag{2}$$

where $\hat{\beta}(u_i, v_i)$ represents the local coefficients to be estimated at location (u_i, v_i); x and y are the vectors of the explanatory and dependent variables, respectively; and $W(u_i, v_i)$ is the weight matrix. In this study, the GWR model was conducted using GWR 4.0 software (https://gwrtools.github.io/category/gwr.html).

The GWRK represents the spatial interpreter that combines GWR and kriging residuals (Kumar et al, 2012; Kumar, 2015). Specifically, residuals from the GWR were kriged and added to the regression estimation to improve prediction accuracy. The equation used to perform GWRK is shown below (Harris et al., 2010; Kumar et al, 2012; Kumar, 2015):

$$y_{gwrk}(u_i, v_i) = y_{gwr}(u_i, v_i) + \varepsilon_{ok}(u_i, v_i) \quad i = 1, 2, \cdots, n \tag{3}$$

where $y_{gwrk}(u_i, v_i)$ is the estimated value at location (u_i, v_i), $y_{gwr}(u_i, v_i)$ is the drift fitted using the GWR model in Equation (1), and $\varepsilon_{ok}(u_i, v_i)$ are the residual values, if these residuals were spatially correlated, Ordinary Kriging (OK) (Goovaerts, 2000; Lloyd, 2005) was used to model the residual values across the study area. Global Moran's I was calculated for the residuals from the GWR model. Moran's I is a commonly used indicator of spatial autocorrelation, it varies from −1 (high negative spatial autocorrelation) to +1 (high positive spatial autocorrelation). A zero value indicates a random spatial pattern (Ishizawa and Stevens, 2007).

2.3.3 Calibration of downscaled precipitation

In this study, the GRA method was employed to calibrate the downscaled precipitation (Vilaet al. 2009;

Duan and Bastiaanssen, 2013). The GRA method is defined as follows:

$$p_{cal} = p_{down} \times (p^{i}_{obs} / p^{i}_{down}) \quad (4)$$

where p_{cal} is the calibrated precipitation, p_{down} is the downscaled precipitation based on the GWRK method. p^{i}_{obs}/p^{i}_{down} represent the ratios between the measurements from the RGS and downscaled precipitation values.

First, the ratios between the measurements from the RGSs and the downscaled precipitation values were computed. Second, the ratios were interpolated to 1 km resolution using the OK interpolation technique. Finally, the downscaled precipitation was corrected to obtain the final calibrated precipitation by multiplying the ratio layer at 1 km resolution.

2.3.4 Monthly fraction disaggregation from annual precipitation

A simple fraction method derived from the TRMM 3B43 monthly data developed by Duan and Bastiaanssen (2013) was used to disaggregate the downscaled and calibrated annual precipitation into monthly precipitation. The process was as follows:

(1) The monthly fractions were defined as:

$$Fraction_i = TRMMo_i / \sum_{i=1}^{12} TRMMo_i \quad (5)$$

where the $TRMMo_i$ represents the precipitation that occurred during the ith month as estimated from the TRMM 3B43 product, and the denominator is the annual total value.

(2) The 0.25° fractions were further interpolated to 1 km resolution, which is consistent with the downscaled and calibrated annual precipitation using the OK interpolation method.

(3) The annual downscaled precipitation values at 1 km resolution were disaggregated into monthly downscaled precipitation values by multiplying the fraction values layer at 1 km resolution.

2.3.5 Validation

Rain gauge data were used to validate the results of downscaling based on the correlation coefficient (*CC*), root mean square error (*RMSE*), mean absolute error (*MAE*), and *Bias*. These variables were defined as follows:

$$CC = \frac{\sum_{i=1}^{n}(o_i - \overline{o})(p_i - \overline{p})}{\sqrt{\sum_{i=1}^{n}(o_i - \overline{o})^2}\sqrt{\sum_{i=1}^{n}(p_i - \overline{p})^2}} \quad (6)$$

$$RMSE = \sqrt{\frac{\sum_{i=1}^{n}(o_i - p_i)^2}{n}} \quad (7)$$

$$MAE = \frac{\sum_{i=1}^{n}|o_i - p_i|}{n} \quad (8)$$

$$Bias = \frac{\sum_{i=1}^{n}(p_i - o_i)}{\sum_{i=1}^{n} o_i} \times 100\% \quad (9)$$

where p_i were the original or downscaled TRMM precipitation values extracted at the location of the i^{th} rain gauge. o_i were the observed precipitation from the i^{th} rain gauge and n was the number of RGS. In the GWR model comparison, o and p represent the original TRMM precipitation and the predicted precipitation for the models at 0.25° resolution, respectively.

3 Results

3.1 Comparison between TRMM 3B43 product and station-based observed precipitation

The accuracy of the TRMM 3B43 was evaluated using rain gauge data before downscaling analysis. Fig. 3 presents scatter plots of TRMM 3B43 precipitation against rain gauge observations at a monthly scale from 2001 to 2015. It can be seen that the TRMM 3B43 product had a high accuracy with only a slight overestimation in this region. At the yearly scale, the *CC* values for the upstream (0.94) and downstream (0.94) regions were higher than that of the midstream region (0.87). In terms of *Bias*, the upstream, midstream, and downstream regions were 6.7%, 22.6%, and 3.1%, respectively, which indicate that more precise estimations were found for the upstream and downstream regions than the midstream region. The performance of the TRMM 3B43 product was also compared for a seasonal basis. March to October was selected as the wet season, and November to April was selected as the dry season, based on climate in the LRB. From Fig. 3, it can be seen that the TRMM 3B43 product over the downstream region can achieve quite good estimations during the wet seasons and dry seasons. However, the performance over the midstream region was poorer, there being a lower *CC* value and larger *Bias*. Notably, the TRMM product

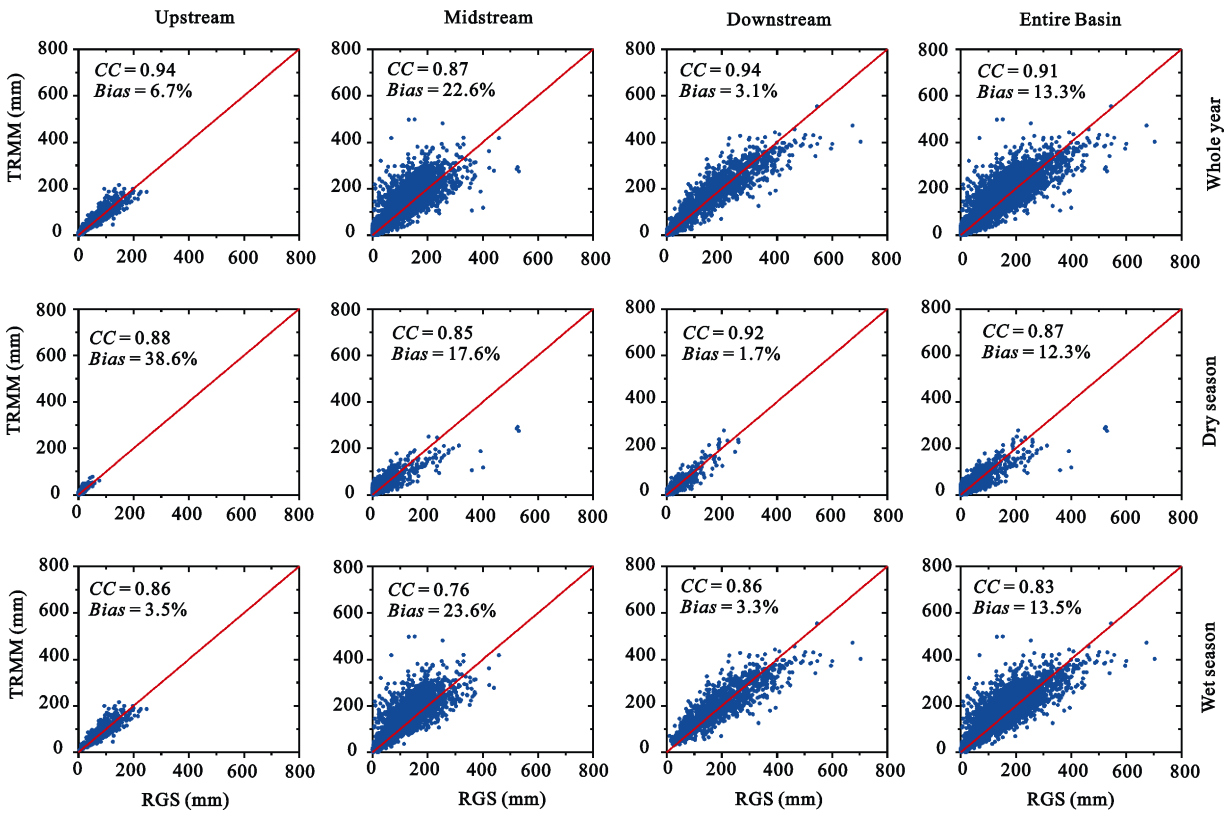

Fig. 3 Scatter plots of Tropical Rainfall Measuring Mission (TRMM) 3B43 precipitation against rainfall gauge station observations at the monthly scale: the three panels show the results from the year (upper panel), dry season (mid panel), and wet season (lower panel). The red line indicates a 1∶1 correspondence. *CC*, correlation coefficient; RGS, rain gauge stations

significantly overestimated the upstream region in the dry season, giving a larger *Bias* (38.6%). Generally, the TRMM 3B43 product was in good agreement with ground observations over this region at the year scale. Spatially, the accuracies for the upstream and downstream region were higher than that of the midstream region.

3.2 Downscaling and calibrating TRMM annual precipitation

The mean annual precipitation data for 2001–2015 were used to demonstrate the applicability of TRMM precipitation downscaling. First, the relationships between the precipitation and environmental variables at the 0.25° scale were analyzed. Fig. 4 presents the spatial distributions of the model parameters and the local coefficients of determination (R^2) generated by the GWR model. It clearly shows that the relationship established at a location may differ greatly from that at other locations. A positive correlation between the TRMM precipitation and NDVI or LST was found over most area of the LRB (Figs. 4c and 4d). However, the correlation between the TRMM precipitation and the topographical factors (i.e., elevation, slope and aspect) obviously showed spatial heterogeneity (Figs. 4b, 4e and 4f), suggesting that the effect of the topography on the precipitation is much more direct and instantaneous compared to the precipitation-NDVI and precipitation-LST relationships (Xu et al., 2015). The local R^2 varies spatially over the study area with an average value of 0.63 (Fig. 4g). The overall performance of the GWR model is shown in Fig. 5. It can be see that the *CC*, *RMSE*, *MAE*, and *Bias* for the GWR model were 0.99, 63 mm, 39 mm and –0.06%, respectively, indicating that the GWR model provided good estimates of TRMM precipitation. Therefore, the GWR was accepted as the function to describe the relationship between the TRMM precipitation and environmental variables.

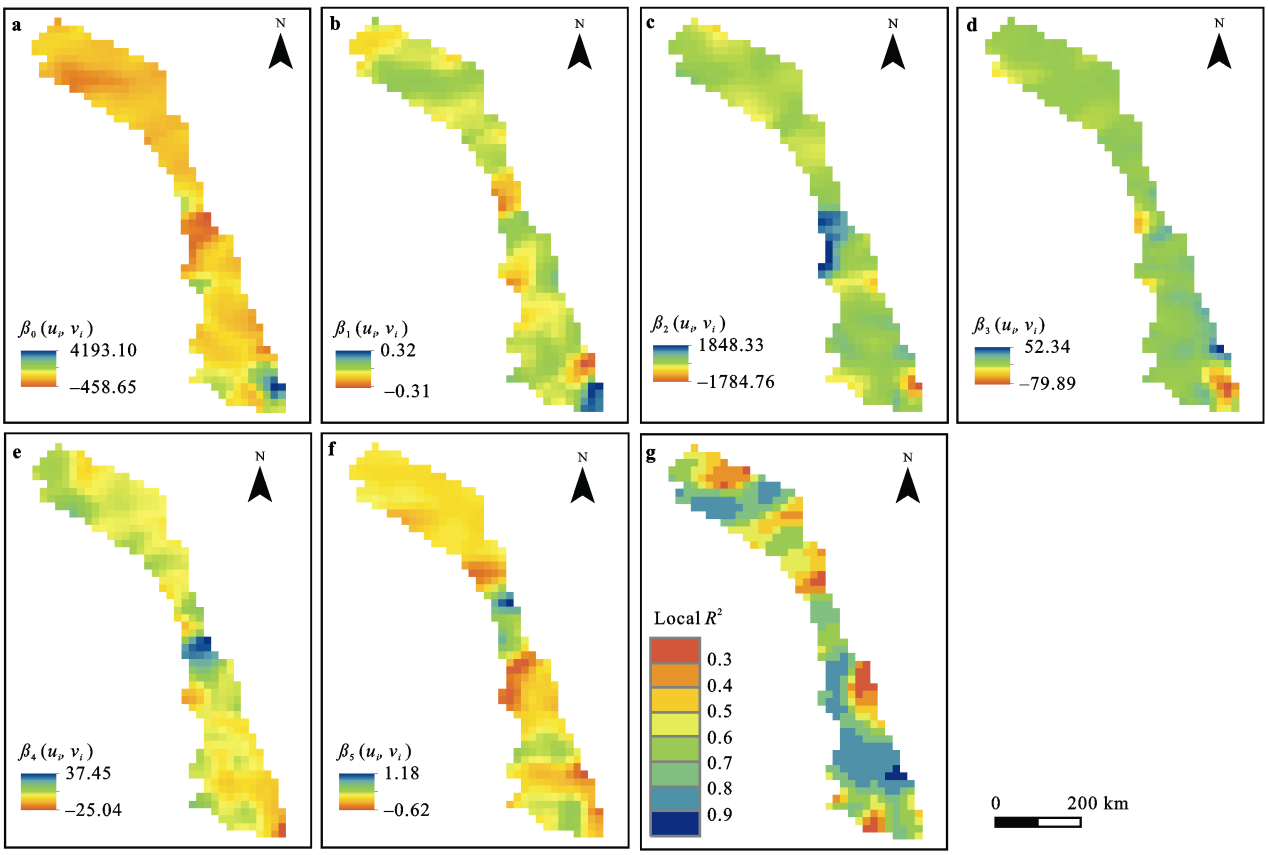

Fig. 4 The spatial pattern of the estimated parameters obtained by the GWR model in the Lancang River Basin. (a) Intercept β_0 (u_i, v_i); (b) slope β_1 (u_i, v_i) for elevation; (c) slope β_2 (u_i, v_i) for NDVI; (d) slope β_3 (u_i, v_i) for LST; (e) slope β_4 (u_i, v_i) for slope; (f) slope β_5 (u_i, v_i) for aspect; and (g) local R^2

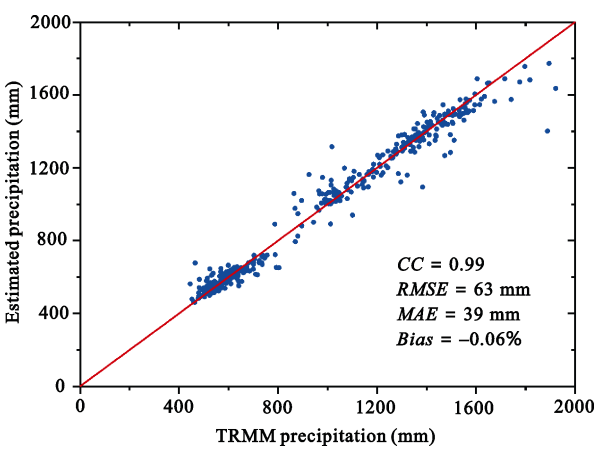

Fig. 5 Scatter plots of Tropical Rainfall Measuring Mission precipitation against estimated precipitation using the GWR model at the 0.25° scale in the Lancang River Basin; The red line indicates a 1 ∶ 1 correspondence. *CC,* correlation coefficient; RGS, rain gauge stations; *RMSE*, root mean square error; *MAE*, mean absolute error

Fig. 6 demonstrates the downscaling and calibration process for TRMM 3B43 precipitation data. Figs. 6a and 6b show similar spatial patterns of estimated TRMM precipitation when compared with the TRMM 3B43 precipitation at a spatial resolution of 0.25°. Fig. 6c shows the spatial distribution of the residuals from the GWR model with a spatial resolution of 0.25°, which were generated by subtracting the predictive values from the original TRMM, and represent the amount of precipitation not explainable with the regression model. Positive values of the residuals indicate that precipitation was underestimated by the GWR method, while negative values indicate overestimation of precipitation. Fig. 6c shows that the overestimated precipitation volumes were mainly in the midstream region, where there was little precipitation due to the fohn effect of the topography. GWR residuals were spatially autocorrelated across the study area and showed a spatial dependence

based on Moran's Index values (Moran's I = 0.06, Z-score = 3.36), which supports the OK approach. Thus, the OK method was used to spatially interpolate precipitation residuals from 0.25° to higher spatial resolution at 1 km (Fig. 6d).

By putting the environmental variables at 1 km resolution into the GWR model established at 0.25° resolution, the predictive annual precipitation at 1 km resolution was obtained. Fig. 6e shows the spatial patterns of the estimated annual precipitation at 1 km resolution. Fig. 6f shows the spatial distribution for the final downscaled TRMM precipitation, which was obtained by adding the estimated annual precipitation at 1 km to the kriging residuals at 1 km obtained previously. From Fig. 6f, the downscaled TRMM precipitation adequately represented observed precipitation patterns. Specifically, high precipitation occurred primarily in the downstream region, and less precipitation was found in the upstream region. Downscaled TRMM precipitation using environmental factors based on the GWRK model better described the spatial patterns of precipitation; there are more details at 1 km spatial resolution when compared with the TRMM 3B43 precipitation.

Calibration with rain gauge data is an essential step to evaluate bias in the downscaled precipitation, which was introduced by the inherent error in the original TRMM precipitation during downscaling (Immerzeel et al., 2009). Duan and Bastiaanssen (2013) reported that both GDA and GRA can improve the accuracy of downscaled precipitation datasets. According to Vila et al. (2009), the GDA method showed large differences for large distinctions between satellite-based and ground-based precipitation data. From the comparison between the original TRMM precipitation and the RGS data (Fig. 3), the TRMM precipitation had a high accuracy with a slight overestimation at the basin scale, i.e., CC = 0.91 and $Bias$ = 13.3%; however, spatially, the $Bias$ of the midstream region reached 22.6%, suggesting a large distinction occurred between the TRMM 3B43 precipitation and the ground-based precipitation. Therefore, the GRA method was used to correct the bias in the downscaled precipitation data using rainfall data from the RGS.

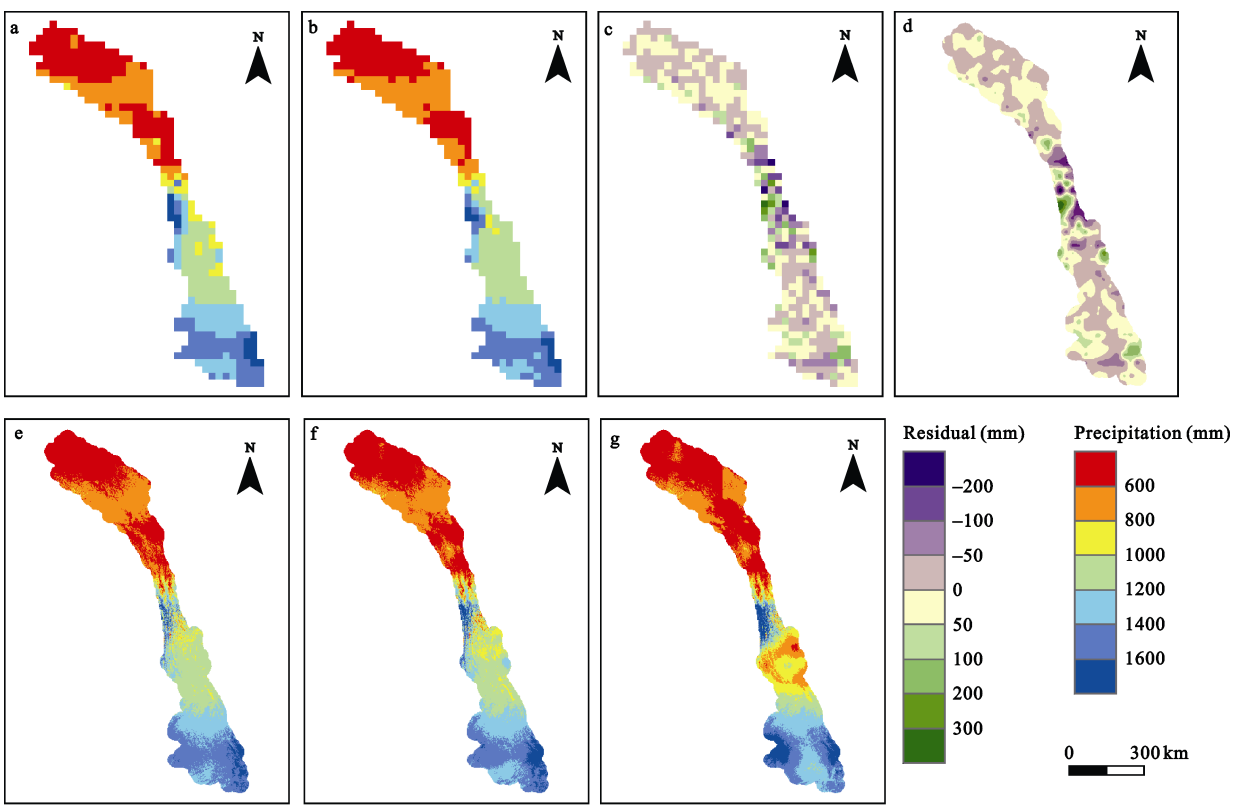

Fig. 6 Downscaled results at 1 km resolution in the Lancang River Basin: (a) Tropical Rainfall Measuring Mission (TRMM) 3B43 precipitation at 0.25° resolution; (b) estimated TRMM precipitation at 0.25° resolution using GWR; (c) GWR residuals at 0.25° resolution; (d) GWR residuals at 1 km resolution; (e) estimated TRMM precipitation at 1 km resolution; (f) downscaled precipitation at 1 km resolution; and (g) calibrated precipitation at 1 km resolution

For the RGS data, a half set was used for calibration and the remaining half set was used for validation. The RGS was separated for calibration and validation as follows: all available 15-year period (2001–2015) average annual precipitation data from all 42 RGS were first calculated and sorted in lowest-highest sequence 1–42; then 20 RGS with odd numbers from 1 to 39 plus number 42 were considered as calibration RGS; the others were validation RGS. This separation forces the calibration to cover the whole range of precipitation, including the lowest and highest values (Duan and Bastiaanssen, 2013). Fig. 6g presents the calibrated precipitation using the GRA method based on calibration RGS. The statistical results for validation are listed in Table 1. The validation results indicated that, compared with the original TRMM 3B43 precipitation, the downscaled precipitation had improved accuracy with reduced *RMSE* and *Bias* values. Moreover, the GRA calibration method can further improve accuracy with increased *CC* and reduced *RMSE*, *MAE,* and *Bias* values. Notably, the LRB is a poorly gauged area with 21 rain gauges for calibration over a 164 800 km^2 area, and hence one gauge represents approximately 7847 km^2. The scarcity of rain gauge stations inevitably limits the skills of the GRA calibration method.

3.3 Monthly results of disaggregating annual precipitation

The previous section demonstrated that the annual precipitation data were obtained at a spatial resolution of 1 km based on the GWRK approach and the GRA calibration method. Zhang et al. (2015) reported that the NDVI response to precipitation has a time lag over the LRB, which differs across the basin, ranging from 1 to 4 months. This implies that it is unfeasible to use NDVI downscaling method directly for the monthly time scale. Therefore, the accumulated 1 km resolution mean annual precipitation for 2001–2015 was disaggregated into monthly time steps using the fraction specified in Equation (5). The calibration of downscaled monthly precipitation was not conducted in this study because duplicated calibration processes on a monthly scale are unnecessary after calibration on an annual scale given the scarcity of available RGS (Duan and Bastiaanssen, 2013). Fig. 7 shows the downscaled monthly precipitation with 1 km resolution. The spatial distribution changes in downscaled monthly precipitation clearly reflect the influence of monsoon activities (both onset and retreat) on precipitation.

The downscaled average monthly precipitation was validated against station-based observed precipitation. Figs. 8a and 8b compare monthly precipitation from 21 validation RGS with the corresponding values from the original TRMM 3B43 data and downscaled monthly data. The TRMM 3B43 data give an estimate of the monthly precipitation with CC = 0.95, $RMSE$ = 30 mm, MAE = 19 mm, and $Bias$ = 14.94%. The CC for the downscaled monthly data was 0.95, while the *RMSE*, *MAE*, and *Bias* decreased to 25 mm, 16 mm, and 0.67%, respectively, indicating the disaggregated 1 km monthly precipitation both improved the spatial resolution, and produced better agreement with the rain gauge data. Considering the strong seasonality of precipitation in this region, the seasonal bias in the TRMM 3B43 data may be introduced into the downscaled monthly precipitation using the monthly fraction disaggregation method. To explore the effect of seasonal bias on the downscaled monthly precipitation, we compared monthly precipitation from the RGS with the TRMM3B43 data and downscaled monthly precipitation data for the dry and wet seasons, respectively. Figs. 8c and 8e show an overestimation of the original TRMM data in both the dry and wet seasons, where *Bias* values were 16.36% and 14.69%, respectively. The *Bias* values for downscaled monthly precipitation were –1.01% in the dry season and 0.97% in the wet season (Figs. 8d and 8f), which indicate that the downscaled monthly precipitation data reduce *Bias* for TRMM 3B43 precipitation in both the dry and wet seasons.

Table 1 Statistics for the validation results using 21 validation rain gauge stations (RGS) in the Lancang River Basin

Datasets	Resolutions	Mean (mm)	*CC*	*RMSE* (mm)	*MAE* (mm)	*Bias* (%)
RGS	—	1012	—	—	—	—
TRMM 3B43	0.25°	1163	0.58	269	181	14.94
Downscaled precipitation	1 km	1120	0.57	253	192	10.66
Calibrated precipitation	1 km	1020	0.75	182	142	0.78

Notes: *CC,* correlation coefficient; *RMSE*, root mean square error; *MAE*, mean absolute error

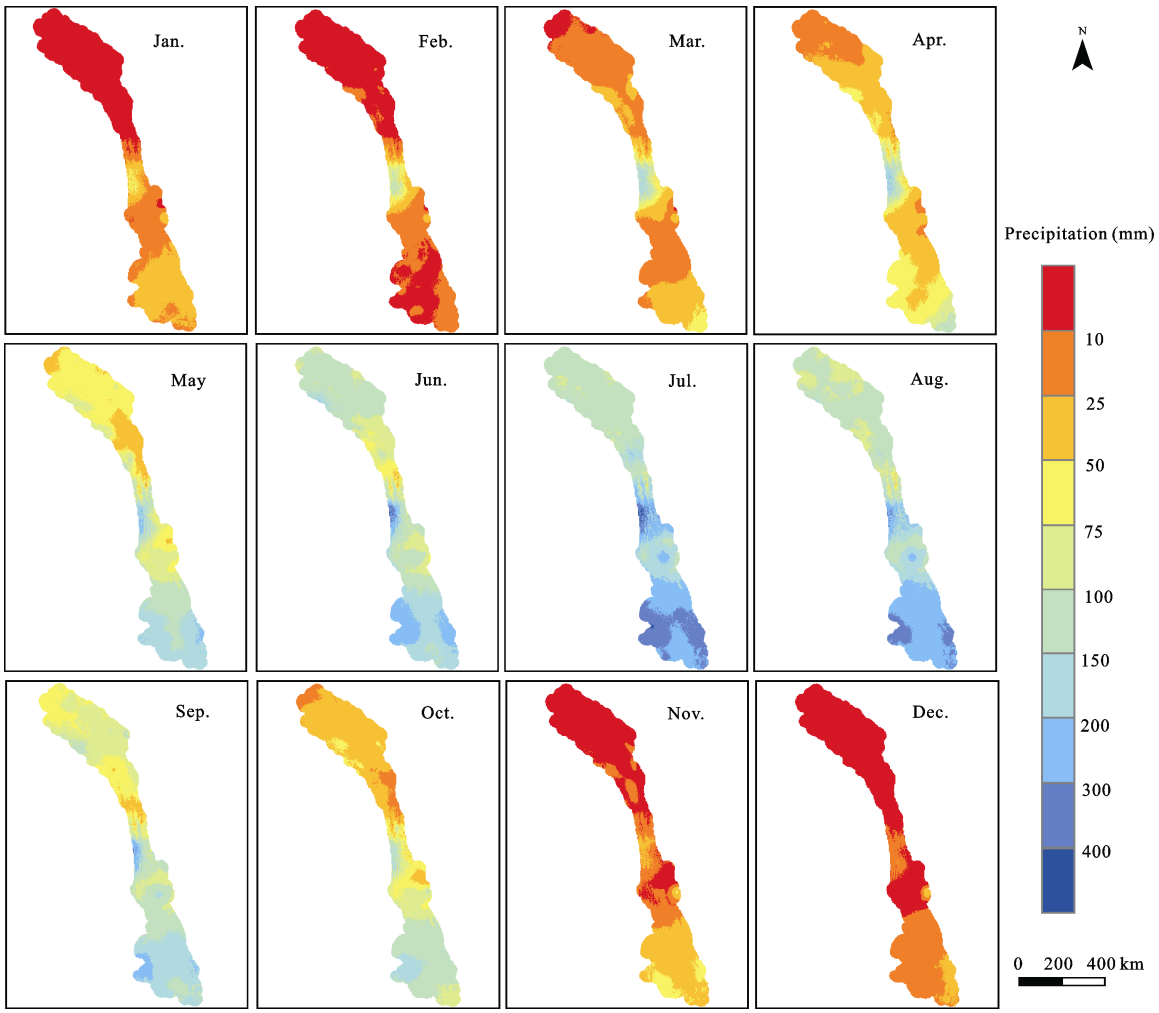

Fig. 7 Downscaled average monthly precipitation for 2001–2015 at 1 km resolution in the Lancang River Basin

4 Discussion

4.1 The relationships between precipitation and environmental variables

Topography can influence regional atmospheric circulation and spatial patterns of precipitation through thermal and dynamic forcing mechanisms (Yin et al., 2008; Guan et al., 2009). In theory, an increase in elevation could increase the relative humidity of air masses by expansion and cooling as the air masses rise, resulting in precipitation (Sokol and Bližňák, 2009). Meanwhile, the spatial pattern of precipitation is also largely dependent on terrain fluctuations, i.e. aspect and slope (Jing et al., 2016). In addition, the responses of vegetation to precipitation are widely acknowledged (Wang et al., 2001; Zhang et al., 2015; Barbosa and Lakshmi Kumar, 2016). Therefore, extensive studies have been devoted to downscaling satellite-based precipitation datasets based on the relationships between precipitation and environmental variables such as DEM and NDVI (Table 2). Moreover, the spatial distribution of precipitation is influenced by other land surface characteristics. For example, co-variability of surface temperature and precipitation is observed globally (Trenberth and Shea, 2005). Schultz and Halpert (1995) found that coupling LST with the NDVI improved the precision and accuracy compared with using NDVI alone in simulating precipitation at a global scale. Thus, considering the LST as an environmental variable may be beneficial for improving the spatial downscaling accuracy of satellite precipitation datasets (Jing et al., 2016; Ma et al., 2017b). In this study, the usage of DEM, NDVI and LST as explanatory variables provided reasonable simulation of the TRMM precipitation, and thus it was feasible to downscale the TRMM precipitation over the LRB. Because atmospheric variables, e.g., relative humidity and

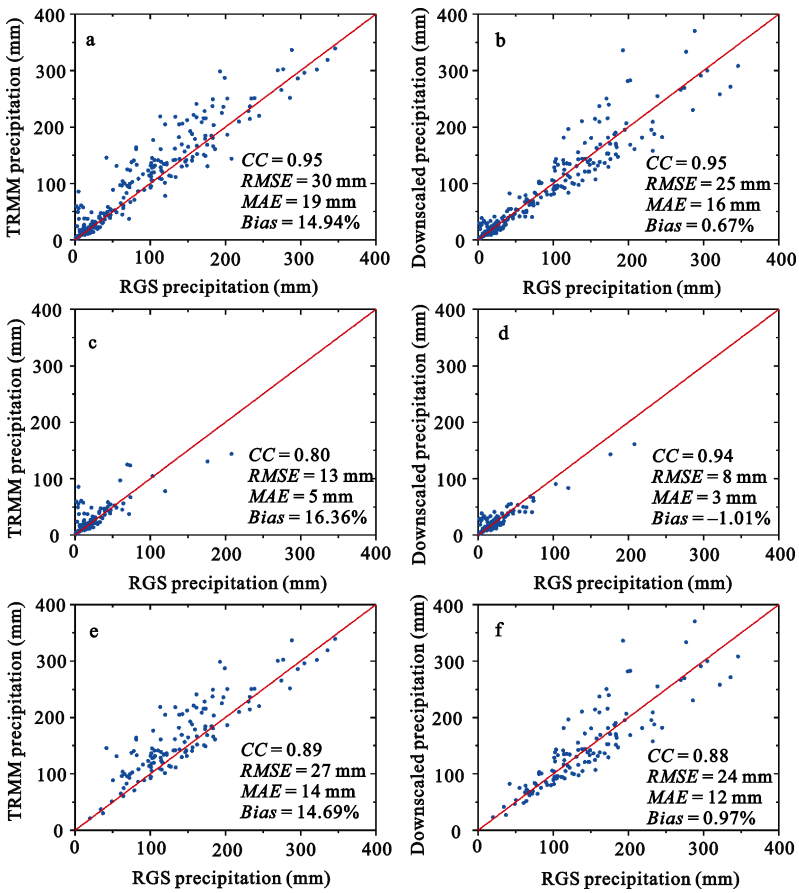

Fig. 8 Comparison of monthly precipitation measured at 21 validation rain gauge stations (RGS) with (a) monthly Tropical Rainfall Measuring Mission (TRMM) 3B43 data; (b) downscaled monthly data; (c) monthly TRMM data in the dry season; (d) downscaled monthly data in the dry season; (e) monthly TRMM data in the wet season; and (f) downscaled monthly data in the wet season. The red line indicates a 1∶1 correspondence. *CC,* correlation coefficient; RGS, rain gauge stations; *RMSE*, root mean square error; *MAE*, mean absolute error

Table 2 Overview of spatial downscaling studies of satellite-based precipitation products

Reference	Environmental variables	Spatial resolution	Temporal scale	Regression models	Regression residual correction method
Immerzeel et al. (2009)	NDVI	0.25° to 1 km	Yearly	Exponential regression	Spline interpolator
Jia et al. (2011)	NDVI and DEM	0.25° to 1 km	Yearly	Multiple linear regression	Spline tension interpolator
Duan and Bastiaanssen (2013)	NDVI	0.25° to 1 km	Yearly	Quadratic function	Spline tension interpolator
Fang et al. (2013)	NDVI, DEM and mete-orological factors	0.25° to 1 km	Hourly	Multiple linear regression	Spline interpolator
Park (2013)	DEM and NDVI	0.25° to 1 km	Monthly	Multiple linear regression	Kriging
Teng et al. (2014)	DEM	0.25° to 1 km	daily	Multiple linear regression	Kriging
Zheng and Zhu (2015)	NDVI and continentality	0.25° to 1 km	Yearly	Multiple linear regression	Inverse distance weighting
Xu et al. (2015)	NDVI and DEM	0.25° to 1 km	Monthly	Geographically weighted regression	Spline tension interpolator
Chen et al. (2014)	NDVI and DEM	0.25° to 1 km	Yearly	Geographically weighted regression	Spline tension interpolator
Zhang et al. (2017)	NDVI	0.25° to 1 km	Yearly	Exponential function	Spline interpolator
Ma et al. (2017a)	NDVI, DEM and LST	0.25° to 1 km	Yearly	a divide-and-conquer method (Cubist)	Spline tension interpolator
Jing et al. (2017)	NDVI, DEM and LST	0.25° to 1 km	Monthly	Support vector machine and random forests	None
Zhang et al. (2018a)	NDVI and DEM	0.25° to 1 km	Monthly	A quadratic parabolic profile (QPP) model	None

Notes: NDVI, Normalized Difference Vegetation Index; LST, Land Surface Temperature; DEM, Digital Elevation Model

wind speed, are closely related to precipitation in the monsoon region, these variables should be considered when downscaling satellite precipitation datasets in the future.

4.2 The downscaling method

Many efforts have been made to develop the downscaling algorithms for satellite-based precipitation (Table 2). As shown in Table 2, the downscaling algorithms based on the exponential regression, quadratic regression and multiple linear regression assume that the relationship between precipitation and environmental variables is constant in space. However, the relationship between precipitation and land surface characteristics is spatially varying (Foody, 2003; Xu et al., 2015). Therefore, the downscaling algorithms based on a global regression model have limitations in those regions with complex topography-atmosphere interactions. Recently, some downscaling algorithms (i.e., GWR, Cubist and QPP), which consider the non-stationarity relationship between precipitation and land surface characteristics, were introduced to downscale satellite-based precipitation (Table 2). These downscaling algorithms may provide better estimates of precipitation than global regression methods such as exponential regression and the multiple linear regression model (Xu et al., 2015; Ma et al., 2017b; Zhang et al., 2018b). In addition, most downscaling algorithms were established using a regression model with residual correction (Table 2). Therefore, residual correction is important for solving the unexplained variation in the regression model and for improving the accuracy of precipitation estimates (Zheng and Zhu, 2015). Park (2013) indicated if reasonable spatial correlation structures are observed in the residuals, this correlation information could improve the quality of the downscaling. In this study, we applied the GWRK model to downscale the TRMM precipitation, which combine the individual strengths of the GWR and the kriging method. Specifically, the GWRK model takes into account the spatial non-stationarity coupled with spatial autocorrelation of the residuals. Our results showed that the performance of the GWRK both improved the spatial resolution of TRMM precipitation and agreed well with observed data from RGS (Fig. 6 and Table 1), indicating this approach can generate reliable precipitation estimates, especially in those regions where precipitation is highly variable spatially.

4.3 Spatial pattern of precipitation over the Lancang River Basin

The LRB is located in the Longitudinal Range-gorge Region (LRGR) in Southwest China (He et al., 2007a). The topography of the LRGR is characterized by longitudinal mountain ranges and deep valleys, which has a 'corridor' effect in the south-north direction and a 'barrier' effect in the east-west direction with respect to the transportation of the southwest and southeast monsoon (He et al., 2005; Wu et al., 2012; Pan et al. 2012). Under the "corridor–barrier" effect of the terrain, surface water vapor, precipitation and runoff over the LRGR exhibited regional differences (Cao et al., 2005; You et al., 2006; He et al., 2007b; Li et al., 2008). Many studies have investigated the temporal and spatial variability of precipitation based on the observed precipitation data at meteorological stations across the LRB (He and Zhang, 2004; Shi et al., 2013; Chen et al., 2017). However, it is difficult to determine accurate spatial distributions of precipitation in such a complex topography and monsoon-affected area due to the lack of a sufficient number of meteorological stations. In contrast, the downscaled TRMM precipitation data at fine spatial resolution in this study effectively captured the high spatial variability of precipitation, which can be used to better explore the 'corridor-barrier' phenomenon. As shown in Fig. 6g, given that the river valley acts as the transportation passage way for warm and wet vapor from south to north, abundant precipitation is observed in the river valley in the southern region. Meanwhile, with the influences of the southwest and southeast monsoon weakening gradually from south to north, the precipitation decreases along the same direction. In addition, the longitudinal mountains act as a barrier to vapor from the southwest and the southeast monsoon, resulting in a spatial pattern where there is more precipitation in the windward side and less in the leeward side. As shown in Fig.7, the effect of the 'corridor-barrier' on the precipitation pattern is more pronounced in the wet season than in the dry season. Generally, the downscaled satellite-based precipitation datasets with high spatial resolution better depict the spatial pattern with more detail, which can provide an alternative to other precipitation datasets for poorly-gauged and inaccessible transboundary river basins.

5 Conclusions

This study investigated a spatial downscaling algorithm

for TRMM 3B43 precipitation to consider non-stationary relationships between precipitation and environmental variables over the LRB. The following conclusions were drawn:

(1) Comparisons between TRMM 3B43 precipitation and observations from rain gauge stations indicated that the TRMM precipitation had a high accuracy with slight overestimation at the basin scale, i.e., *CC* = 0.91 and *Bias* = 13.3%. Spatially, the accuracies of the upstream and downstream regions were higher than that of the midstream region.

(2) The GWRK approach assumes that the relationship between precipitation and environmental variables varies spatially, which is in agreement with the actual situation. The downscaling results obtained using the GWRK approach effectively captured the high spatial variability of precipitation over the LRB. Moreover, the downscaled precipitation with high spatial resolution better depicted the precipitation pattern influenced by the interaction of topography and monsoon over this region.

(3) Calibration with rain gauge data is an essential step for downscaling precipitation data. The annual downscaled TRMM precipitation using GRA calibration can further improve the accuracy when compared with the original TRMM dataset, i.e., *CC* = 0.75, *RMSE* = 182 mm, *MAE* = 142 mm, and *Bias* = 0.78%.

(4) The simple disaggregation method based on monthly fractions was used to disaggregate annual precipitation to 1 km monthly precipitation. The disaggregated 1 km monthly precipitation improved the spatial resolution, and also agreed well with rain gauge data when compared with the original TRMM precipitation, i.e., *CC* = 0.95, *RMSE* = 25 mm, *MAE* = 16 mm, and *Bias* = 0.67%.

References

Barbosa H A, Lakshmi Kumar T V, 2016. Influence of rainfall variability on the vegetation dynamics over Northeastern Brazil. *Journal of Arid Environments*, 124: 377–387. doi: 10.1016/j.jaridenv.2015.08.015

Bohnenstengel S I, Schlünzen K H, Beyrich F, 2011. Representativity of in situ precipitation measurements – A case study for the LITFASS area in North-Eastern Germany. *Journal of Hydrology*, 400(3–4): 387–395. doi: 10.1016/j.jhydrol.2011.01. 052

Cao Jie, He Daming, Yao Ping, 2005. Research on the spatial distribution of rainfall and temperature in winter and summer over longitudinal range-gorge region (LRGR). *Advances in Earth Science*, 20(11): 1176–1182. (in Chinese)

Chen F R, Liu Y, Liu Q et al., 2014. Spatial downscaling of TRMM 3B43 precipitation considering spatial heterogeneity. *International Journal of Remote Sensing*, 35(9): 3074–3093. doi: 10.1080/01431161.2014.902550

Chen Sujing, Li Lijuan, Li Jiuyi et al., 2017. Analysis of the temporal and spatial variation characteristics of precipitation in the Lancang River Basin over the past 55 years. *Journal of Geo–information Science*, 19(3): 365–373. (in Chinese)

Derin Y, Anagnostou E, Berne A et al., 2016. Multiregional satellite precipitation products evaluation over complex terrain. *Journal of Hydrometeorology*, 17(6): 1817–1836. doi: 10. 1175/jhm-d-15-0197.1

Duan Z, Bastiaanssen W G M, 2013. First results from Version 7 TRMM 3B43 precipitation product in combination with a new downscaling–calibration procedure. *Remote Sensing of Environment*, 131: 1–13. doi: 10.1016/j.rse.2012.12.002

Fang J, Du J, Xu W et al., 2013. Spatial downscaling of TRMM precipitation data based on the orographical effect and meteorological conditions in a mountainous area. *Advances in Water Resources*, 61: 42–50. doi: 10.1016/j.advwatres.2013.08. 011

Foody G M, 2003. Geographical weighting as a further refinement to regression modelling: an example focused on the NDVI–rainfall relationship. *Remote Sensing of Environment*, 88(3): 283–293. doi: 10.1016/j.rse.2003.08.004

Fotheringham A S, Brunsdon C, Charlton M, 2002. *Geographically Weighted Regression: The Analysis of Spatially Varying Relationships*. New York: Wiley.

Gao Y, Huang J, Li S et al., 2012. Spatial pattern of non- stationarity and scale-dependent relationships between NDVI and climatic factors—A case study in Qinghai-Tibet Plateau, China. *Ecological Indicators*, 20: 170–176. doi: 10.1016/ j.ecolind.2012.02.007

Goovaerts P, 2000. Geostatistical approaches for incorporating elevation into the spatial interpolation of rainfall. *Journal of Hydrology*, 228(1–2): 113–129. doi: 10.1016/S0022-1694(00) 00144-X

Guan H D, Wilson J L, Xie H J, 2009. A cluster-optimizing regression-based approach for precipitation spatial downscaling in mountainous terrain. *Journal of Hydrology*, 375(3–4): 578–588. doi: 10.1016/j.jhydrol.2009.07.007

Harris P, Fotheringham A S, Crespo R et al., 2010. The use of geographically weighted regression for spatial prediction: an evaluation of models using simulated data sets. *Mathematical Geosciences*, 42(6): 657–680. doi: 10.1007/s11004-010-9284-7

He Daming, Wu Shaohong, Peng Hua et al., 2005. A study of ecosystem changes in Longitudinal Range-Gorge Region and transboundary eco-security in Southwest China. *Advances in Earth Science*, 20(3): 338–344. (in Chinese)

He Daming, Liu Jiang, Hu Jinming et al., 2007a. Transboundary eco-security and its regulation system in the Longitudinal Range-Gorge Region. *Chinese Science Bulletin*, 52(S2): 1–9. doi: 10.1007/s11434-007-7001-9

He Daming, Li Shaojuan, Zhang Yiping, 2007b. The variation

and regional differences of precipitation in the Longitudinal Range-Gorge the Region. *Chinese Science Bulletin*, 52(S2): 59–73. doi: 10.1007/s11434-007-7007-3

He Daming, Feng Yan, Hu Jingming, 2007c. *Utilization of Water Resources and Environmental Conservation in the Internation Rivers, Southwest China*. Beijing: Science Press. (in Chinese)

He Yunling, Zhang Yiping, 2004. The climate characteristics and change trends on basins of Lancangjiang valley in Yunnan Province. *Journal of Mountain Science*, 22(5): 539–548. (in Chinese)

He Z H, Yang L, Tian F Q et al., 2017. Intercomparisons of rainfall estimates from TRMM and GPM multisatellite products over the Upper Mekong River Basin. *Journal of Hydrometeorology*, 18(2): 413–430. doi: 10.1175/jhm-d-16-0198.1

Hou A Y, Kakar R K, Neeck S et al., 2014. The global precipitation measurement mission. *Bulletin of the American Meteorological Society*, 95(5): 701–722. doi: 10.1175/bams-d-13-00164.1

Huffman G J, Adler R F, Arkin P et al., 1997. The Global Precipitation Climatology Project (GPCP) combined precipitation dataset. *Bulletin of the American Meteorological Society*, 78(1): 5–20. doi: 10.1175/1520-0477(1997)078<0005: tgpcpg>2.0.co;2

Huffman G J, Bolvin D T, Nelkin E J et al., 2007. The TRMM Multisatellite Precipitation Analysis (TMPA): quasi-global, multiyear, combined-sensor precipitation estimates at fine scales. *Journal of Hydrometeorology*, 8(1): 38–55. doi: 10.1175/jhm560.1

Immerzeel W W, Rutten M M, Droogers P, 2009. Spatial downscaling of TRMM precipitation using vegetative response on the Iberian Peninsula. *Remote Sensing of Environment*, 113(2): 362–370. doi: 10.1016/j.rse.2008.10.004

Imran M, Stein A, Zurita-Milla R, 2015. Using geographically weighted regression kriging for crop yield mapping in West Africa. *International Journal of Geographical Information Science*, 29(2): 234–257. doi: 10.1080/13658816.2014.959522

Ishizawa H, Stevens G, 2007. Non-english language neighborhoods in Chicago, Illinois: 2000. *Social Science Research*, 36(3): 1042–1064. doi: 10.1016/j.ssresearch.2006.06.005

Jia S F, Zhu W B, Lű A F et al., 2011. A statistical spatial downscaling algorithm of TRMM precipitation based on NDVI and DEM in the Qaidam Basin of China. *Remote Sensing of Environment*, 115(12): 3069–3079. doi: 10.1016/j.rse.2011.06.009

Jing W L, Yang Y P, Yue X F et al., 2016. A comparison of different regression algorithms for downscaling monthly satellite-based precipitation over North China. *Remote Sensing*, 8(10): 835. doi: 10.3390/rs8100835

Jing W L, Zhang P Y, Jiang H et al., 2017. Reconstructing satellite-based monthly precipitation over Northeast China using machine learning algorithms. *Remote Sensing*, 9(8): 781. doi: 10.3390/rs9080781

Joyce R J, Janowiak J E, Arkin P A et al., 2004. CMORPH: a method that produces global precipitation estimates from passive microwave and infrared data at high spatial and temporal resolution. *Journal of Hydrometeorology*, 5(3): 487–503. doi: 10.1175/1525-7541(2004)005<0487:CAMTPG>2.0.CO;2

Kumar S, Lal R, Liu D S, 2012. A geographically weighted regression kriging approach for mapping soil organic carbon stock. *Geoderma*, 189–190: 627–634. doi: 10.1016/j. geoderma.2012.05.022

Kumar S, 2015. Estimating spatial distribution of soil organic carbon for the Midwestern United States using historical database. *Chemosphere*, 127: 49–57. doi: 10.1016/j.chemosphere. 2014.12.027

Lauri H, Räsänen T A, Kummu M, 2014. Using reanalysis and remotely sensed temperature and precipitation data for hydrological modeling in monsoon climate: Mekong River case study. *Journal of Hydrometeorology*, 15(4): 1532–1545. doi: 10.1175/jhm-d-13-084.1

Li B, Tao S, Dawson R W, 2002. Relations between AVHRR NDVI and ecoclimatic parameters in China. *International Journal of Remote Sensing*, 23(5): 989–999. doi: 10.1080/014311602753474192

Li Y G, He D M, Ye C Q, 2008. Spatial and temporal variation of runoff of Red River Basin in Yunnan. *Journal of Geographical Sciences*, 18(3): 308–318. doi: 10.1007/s11442-008-0308-x

Liu X M, Yang T T, Hsu K et al., 2017. Evaluating the streamflow simulation capability of PERSIANN-CDR daily rainfall products in two river basins on the Tibetan Plateau. *Hydrology and Earth System Sciences*, 21(1): 169–181. doi: 10.5194/hess-21-169-2017

Lloyd C D, 2005. Assessing the effect of integrating elevation data into the estimation of monthly precipitation in Great Britain. *Journal of Hydrology*, 308(1–4): 128–150. doi: 10.1016/j.jhydrol.2004.10.026

Ma Z Q, Shi Z, ZhouY et al., 2017a. A spatial data mining algorithm for downscaling TMPA 3B43 V7 data over the Qinghai–Tibet Plateau with the effects of systematic anomalies removed. *Remote Sensing of Environment*, 200: 378–395. doi: 10.1016/j.rse.2017.08.023

Ma Z Q, Zhou Y, Hu B F et al., 2017b. Downscaling annual precipitation with TMPA and land surface characteristics in China. *International Journal of Climatology*, 37(15): 5107–5119. doi: 10.1002/joc.5148

Meersmans J, Van Weverberg K, De Baets S et al., 2016. Mapping mean total annual precipitation in Belgium, by investigating the scale of topographic control at the regional scale. *Journal of Hydrology*, 540: 96–105. doi: 10.1016/j.jhydrol. 2016.06.013

Miao C Y, Ashouri H, Hsu K L et al., 2015. Evaluation of the PERSIANN-CDR daily rainfall estimates in capturing the behavior of extreme precipitation events over China. *Journal of Hydrometeorology*, 16(3): 1387–1396. doi: 10.1175/jhm-d-14-0174.1

Michaelides S, Levizzani V, Anagnostou E et al., 2009. Precipitation: measurement, remote sensing, climatology and modeling. *Atmospheric Research*, 94(4): 512–533. doi: 10.1016/j.atmosres.2009.08.017

Pan Tao, Wu Shaohong, He Daming et al., 2012. Effects of longitudinal range-gorge terrain on the eco-geographical pattern in Southwest China. *Journal of Geographical Sciences*, 22(5):

825–842. doi: 10.1007/s11442-012-0966-6

Park N W, 2013. Spatial downscaling of TRMM precipitation using geostatistics and fine scale environmental variables. *Advances in Meteorology*, 2013: Article ID 237126. doi: 10.1155/2013/237126

Prakash S, Mitra A K, AghaKouchak A et al., 2015. Error characterization of TRMM Multisatellite Precipitation Analysis (TMPA-3B42) products over India for different seasons. *Journal of Hydrology*, 529: 1302–1312. doi: 10.1016/j.jhydrol.2015.08.062

Prakash S, Mitra A K, AghaKouchak A et al., 2018. A preliminary assessment of GPM-based multi-satellite precipitation estimates over a monsoon dominated region. *Journal of Hydrology*, 556: 865–876. doi: 10.1016/j.jhydrol.2016.01.029

Schultz P A, Halpert M S, 1995. Global analysis of the relationships among a vegetation index, precipitation and land surface temperature. *International Journal of Remote Sensing*, 16(15): 2755–2777. doi: 10.1080/01431169508954590

Shi W L, Yu X Z, Liao W G et al., 2013. Spatial and temporal variability of daily precipitation concentration in the Lancang River basin, China. *Journal of Hydrology*, 495: 197–207. doi: 10.1016/j.jhydrol.2013.05.002

Sokol Z, Bližňák V, 2009. Areal distribution and precipitation–altitude relationship of heavy short-term precipitation in the Czech Republic in the warm part of the year. *Atmospheric Research*, 94(4): 652–662. doi: 10.1016/j.atmosres.2009. 03.001

Sorooshian S, Hsu K L, Gao X G et al., 2000. Evaluation of PERSIANN system satellite–based estimates of tropical rainfall. *Bulletin of the American Meteorological Society*, 81(9): 2035–2046. doi: 10.1175/1520-0477(2000)081<2035:eopsse>2.3.co;2

Teng H F, Shi Z, Ma Z Q et al., 2014. Estimating spatially downscaled rainfall by regression kriging using TRMM precipitation and elevation in Zhejiang Province, southeast China. *International Journal of Remote Sensing*, 35(22): 7775–7794. doi: 10.1080/01431161.2014.976888

Trenberth K E, Shea D J, 2005. Relationships between precipitation and surface temperature. *Geophysical Research Letters*, 32: L14703. doi: 10.1029/2005gl022760

Vila D A, de Goncalves L G G, Toll D L et al., 2009. Statistical evaluation of combined daily gauge observations and rainfall satellite estimates over Continental South America. *Journal of Hydrometeorology*, 10(2): 533–543. doi: 10.1175/ 2008jhm1048.1

Wang J, Price K P, Rich P M, 2001. Spatial patterns of NDVI in response to precipitation and temperature in the central Great Plains. *International Journal of Remote Sensing*, 22(18): 3827–3844. doi: 10.1080/01431160010007033

Wang W, Lu H, Yang D W et al., 2016. Modelling hydrologic processes in the Mekong River Basin using a distributed model driven by satellite precipitation and rain gauge observations. *PLoS One*, 11(3): e0152229. doi: 10.1371/journal.pone.0152229

Wu Shaohong, Pan Tao, Cao Jie et al., 2012. Barrier-corridor effect of longitudinal range-gorge terrain on monsoons in Southwest China. *Geographical Research*, 31(1): 1–13. (in Chinese)

Xu S G, Wu C Y, Wang L et al., 2015. A new satellite-based monthly precipitation downscaling algorithm with non-stationary relationship between precipitation and land surface characteristics. *Remote Sensing of Environment*, 162: 119–140. doi: 10.1016/j.rse.2015.02.024

Yin Z Y, Zhang X Q, Liu X D et al., 2008. An assessment of the biases of satellite rainfall estimates over the Tibetan Plateau and correction methods based on topographic analysis. *Journal of Hydrometeorology*, 9(3): 301–326. doi: 10.1175/2007jhm903.1

You Weihong, Duan Changchun, He Daming, 2006. Climatic difference in dry and wet season under effect of the Longitudinal Range-gorge and its influence on transboundary river runoff. *Chinese Science Bulletin*, 51(S1): 69–79. doi: 10.1007/s11434-006-8069-3

Yuan F, Zhang L M, Win K W W et al., 2017. Assessment of GPM and TRMM multi-satellite precipitation products in streamflow simulations in a data-sparse mountainous watershed in Myanmar. *Remote Sensing*, 9(3): 302. doi: 10.3390/rs9030302

Zeng H W, Li L J, Li J Y, 2012. The evaluation of TRMM Multisatellite Precipitation Analysis (TMPA) in drought monitoring in the Lancang River Basin. *Journal of Geographical Sciences*, 22(2): 273–282. doi: 10.1007/s11442-012-0926-1

Zeng H W, Li L J, Hu J M et al., 2013. Accuracy validation of TRMM Multisatellite Precipitation Analysis daily precipitation products in the Lancang River Basin of China. *Theoretical and Applied Climatology*, 112(3–4): 389–401, doi: 10.1007/s00704-012-0733-8

Zhang Jinghua, Feng Zhiming, Jiang Luguang et al., 2015. Analysis of the correlation between NDVI and climate factors in the Lancang River Basin. *Journal of Natural Resources*, 30(9): 1425–1435. (in Chinese)

Zhang Q, Shi P J, Singh V P et al., 2017. Spatial downscaling of TRMM-based precipitation data using vegetative response in Xinjiang, China. *International Journal of Climatology*, 37(10): 3895–3909. doi: 10.1002/joc.4964

Zhang T, Li B L, Yuan Y C et al., 2018a. Spatial downscaling of TRMM precipitation data considering the impacts of macro-geographical factors and local elevation in the Three-River Headwaters Region. Remote *Sensing of Environment*, 215: 109–127. doi: 10.1016/j.rse.2018.06.004

Zhang Y Y, Li Y G, Ji X et al., 2018b. Fine-resolution precipitation mapping in a mountainous watershed: geostatistical downscaling of TRMM products based on environmental variables. *Remote Sensing*, 10(1): 119. doi: 10.3390/rs10010119

Zhang Y Y, Li Y G, Ji X et al., 2018c. Evaluation and hydrologic validation of three satellite-based precipitation products in the upper catchment of the Red River Basin, China. *Remote Sensing*, 10(12): 1881. doi:10.3390/rs10121881

Zhao H G, Yang B G, Yang S T et al., 2018. Systematical estimation of GPM-based global satellite mapping of precipitation products over China. *Atmospheric Research*, 201: 206–217. doi: 10.1016/j.atmosres.2017.11.005

Zheng X, Zhu J J, 2015. A methodological approach for spatial downscaling of TRMM precipitation data in North China. *International Journal of Remote Sensing*, 36(1): 144–169. doi: 10.1080/01431161.2014.995275

Zhou X, Ni G H, Shen C et al., 2017. Remapping annual precipitation in mountainous areas based on vegetation patterns: a case study in the Nu River basin. *Hydrology and Earth System Sciences*, 21(2): 999–1015. doi: 10.5194/hess-21- 999-2017